Обзор ArXiv: astro-ph, 10-16 мая 2018 года

От Сильченко О.К.

Astro-ph: 1805.03543

UVIT Observations of the Star-Forming Ring in NGC7252: Evidence of Possible AGN Feedback Suppressing Central Star Formation

K. George[1,⋆], P. Joseph[1,2], C. Mondal[1], A. Devaraj[1], A. Subramaniam[1], C. S. Stalin[1], P. Côté[3], S. K. Ghosh[4,5], J. B. Hutchings[3], R. Mohan[1], J. Postma[6], K. Sankarasubramanian[1,7], P. Sreekumar[1], S.N. Tandon[1,8]

[1] Indian Institute of Astrophysics, Koramangala II Block, Bangalore, India
[2] Department of Physics, Christ University, Bangalore, India
[3] National Research Council of Canada, Herzberg Astronomy and Astrophysics Research Centre, Victoria, Canada
[4] National Centre for Radio Astrophysics, Pune, India
[5] Tata Institute of Fundamental Research, Mumbai, India
[6] University of Calgary, Calgary, Alberta Canada
[7] ISRO Satellite Centre, HAL Airport Road, Bangalore, India
[8] Inter-University Center for Astronomy and Astrophysics, Pune, India

May 10, 2018

ABSTRACT

Context. Some post-merger galaxies are known to undergo a starburst phase that quickly depletes the gas reservoir and turns it into a red-sequence galaxy, though the details are still unclear.
Aims. Here we explore the pattern of recent star formation in the central region of the post-merger galaxy NGC7252 using high resolution UV images from the UVIT on ASTROSAT.
Methods. The UVIT images with 1.2 and 1.4 arcsec resolution in the FUV and NUV are used to construct a FUV-NUV colour map of the central region.
Results. The FUV–NUV pixel colour map for this canonical post-merger galaxy reveals a blue circumnuclear ring of diameter ~ 10"

UVIT – ультрафиолетовый телескоп на индийском спутнике

- Две фотометрические полосы, FUV (1480 A) и NUV (2420 A).
- Пространственное разрешение – 1.2 и 1.4 секунды дуги, соответственно.
- Для оценки возрастов звездного населения сворачивали спектры из STARBURST99 со своими кривыми пропускания для обоих фильтров.

Объект исследования NGC 7252

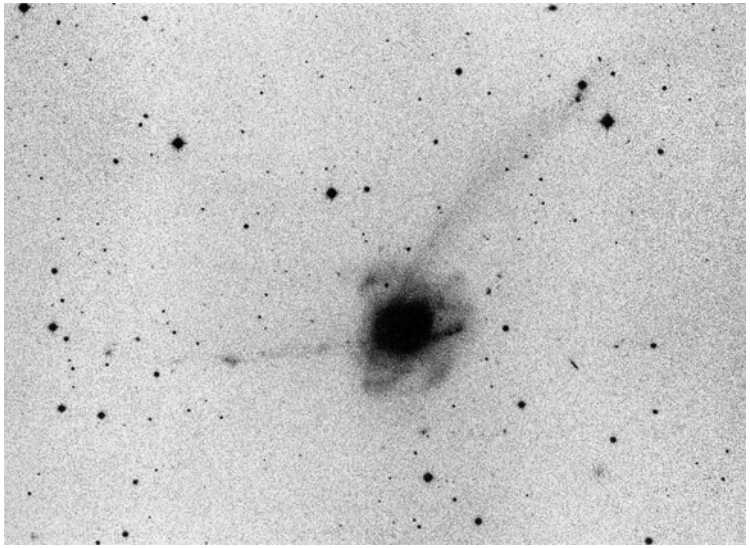

Blue photo

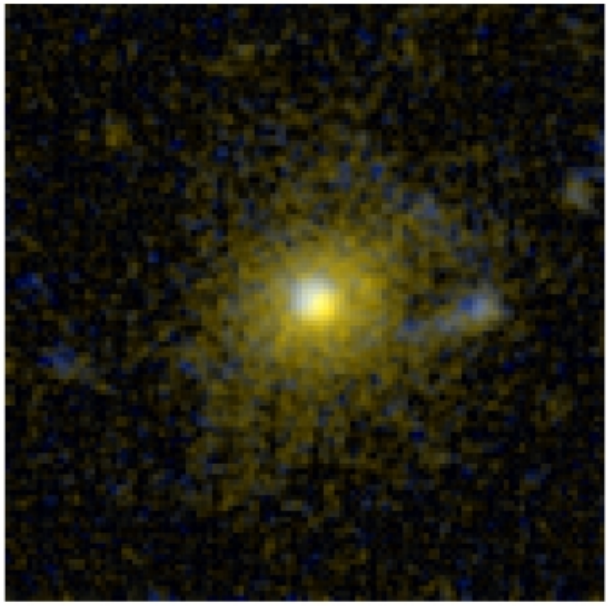

GALEX

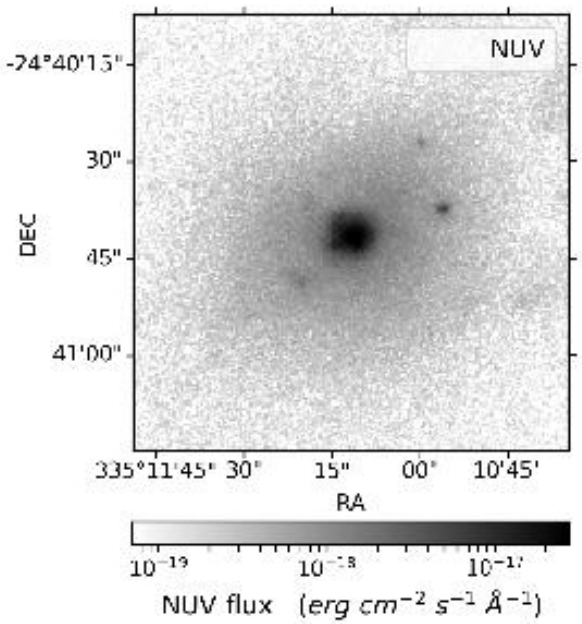
NUV
-24°40'15"
30"
45"
41'00"
DEC
335°11'45" 30"
15"
00"
10'45"
RA
NUV flux (erg cm^{-2} s^{-1} Å^{-1})

(a)

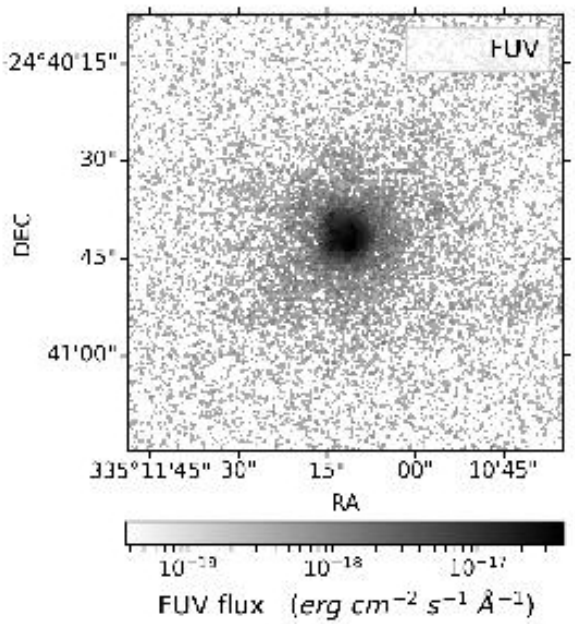
FUV
24°40'15"
30"
45"
41'00"
DEC
335°11'45" 30"
15"
00"
10'45"
RA
FUV flux (erg cm^{-2} s^{-1} Å^{-1})

(b)

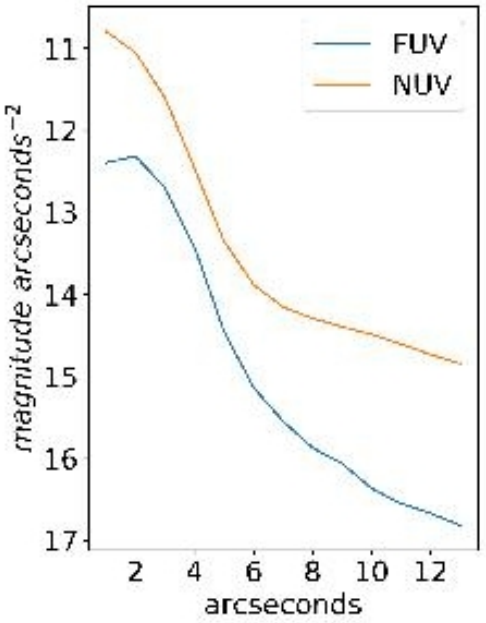
FUV
NUV
11
12
13
14
15
16
17
magnitude arcseconds^{-2}
2
4
6
8
10
12
arcseconds

(c)

Карта цвета FUV-NUV с контурами возрастов

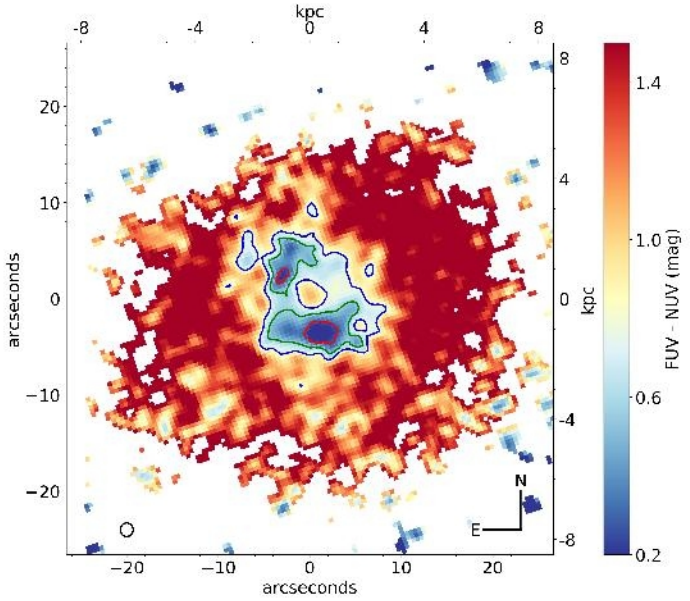

Fig. 2: $FUV - NUV$ colour map of the main body of NGC7252. The pixels are colour coded in units of $FUV - NUV$ colour. The point spread function for UVIT is shown in black circle. The image measures $\sim 50'' \times 50''$ and corresponds to a physical size of ~ 16 kpc on each side. Age contours of 150 (red), 250 (green), 300 (blue) Myr are overlaid over the colour map to isolate regions of constant age. The blue ring is clearly seen with bluer colour clumps. The ring hosts young ($\lesssim 150$ Myr) stellar populations compared to the rest of the galaxy.

Astro-ph: 1805.03842

The XXL Survey: XXX. Characterisation of the XLSSsC N01 supercluster and analysis of the galaxy stellar populations

V. Guglielmo[1,2,3], B. M. Poggianti[1], B. Vulcani[4,1], A. Moretti[1], J. Fritz[5], F. Gastaldello[6], C. Adami[2], C. A. Caretta[7], J.Willis[12], E. Koulouridis[8,9], M. E. Ramos Ceja[11], P. Giles[12], I. Baldry[14], M. Birkinshaw[12], A. Bongiorno[15], M. Brown[16], L. Chiappetti[6], S. Driver[17,18], A. Elyiv[19,20], A. Evrard[21], M. Grootes[22], L. Guennou[23], A. Hopkins[24], C. Horellou[25], A. Iovino[26], S. Maurogordato[27], M. Owers[28], F. Pacaud[11], S. Paltani[29], M. Pierre[8,9], M. Plionis[30,31], T. Ponman[32], A. Robotham[17], T. Sadibekova[33], V. Smolčić[34], R. Tuffs[22], and C. Vignali[10,19]

(Affiliations can be found after the references)

Received xxx; accepted yyy

ABSTRACT

Context. Superclusters form from the largest enhancements in the primordial density perturbation field and extend for tens of Mpc, tracing the large-scale structure of the Universe. X-ray detections and systematic characterisations of superclusters and the properties of their galaxies have only been possible in the last few years.

Aims. We characterise XLSSsC N01, a rich supercluster at z~0.3 detected in the XXL Survey, composed of X-ray clusters of different virial masses and X-ray luminosities. As one of the first studies on this topic, we investigate the stellar populations of galaxies in different environments in the supercluster region.

Methods. We study a magnitude-limited ($r \leq 20$) and a mass-limited sample ($\log(M_*/M_\odot) \geq 10.8$) of galaxies in the virialised region and in the outskirts of 11 XLSSsC N01 clusters, in high-density field regions, and in the low-density field. We compute the stellar population properties of galaxies using spectral energy distribution (SED) and spectral fitting techniques, and study the dependence of star formation rates (SFR), colours, and stellar ages on environment.

Свойства звездного населения в:

- ~ 4000 галактиках на z=0.3,
- из которых ~130 + ~130 принадлежат 11 РЕНТГЕНОВСКИМ скоплениям,
- А остальные – в полях разной плотности.
- Спектры собраны по разным обзорам, к ним прикладывается SINOPSIS – фиттинг суммой 12 SSP разных возрастов.

Разбиение по типу окружения:

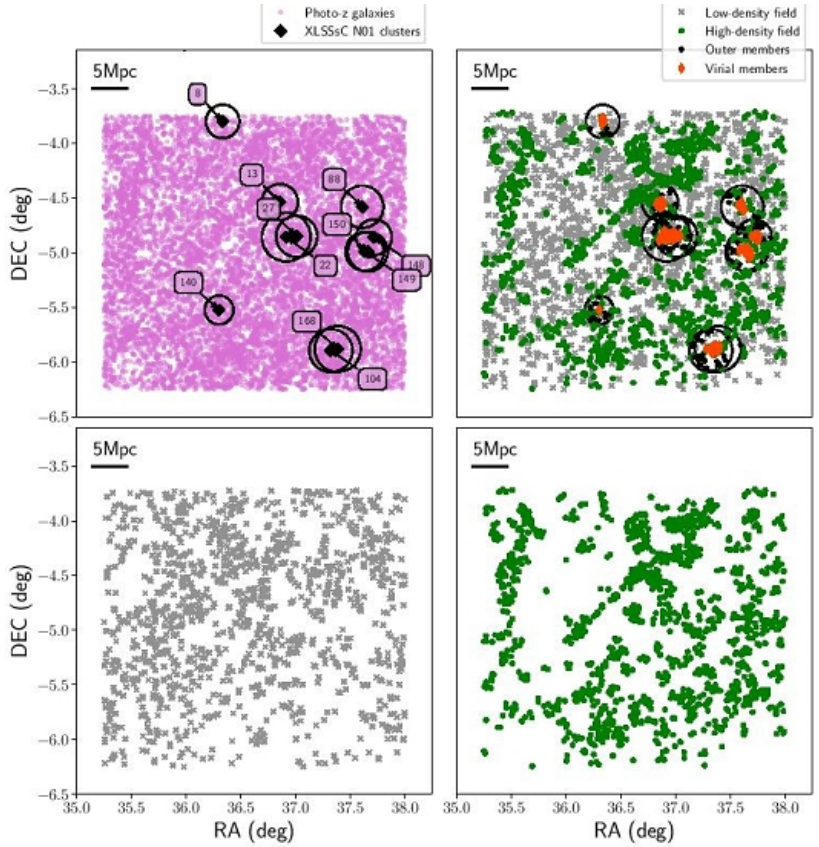

Fig. 1: Sky distribution of galaxies in the XLSSsC N01 supercluster region. Top left: Galaxies with a photo-z redshift in the range between 0.25 and 0.35 and used to compute the LD (black points). Top right: Galaxies with a spectroscopic redshift, colour-coded according to their environment (see Sect. 3). Grey crosses are low-density field galaxies, green dots are high-density field galaxies, dark orange diamonds are virial members, and black stars are outer members. In the top panels, black circles show the projected extension in the sky of 3 r_{200} for each cluster in the superstructure. The two bottom panels show the low- and high-density field samples separately, with the same symbols as the top right panel.

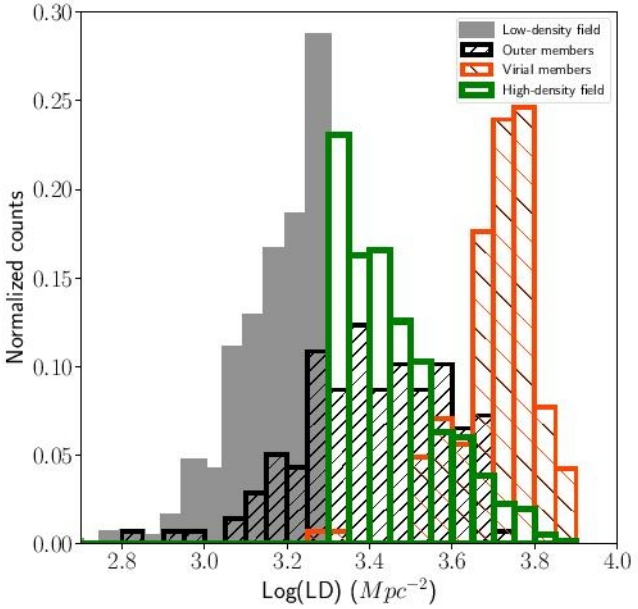

Fig. 2: Normalised local density distribution computed using the photo-z sample in redshift range $0.25 \leq z_{phot} \leq 0.35$. The grey histogram represents the low-density field, the green empty histogram galaxies in the high-density field, the black hatched histogram the cluster outer members, and the orange hatched histogram the cluster virial members.

Разбиение на активные/пассивные (2 способа)

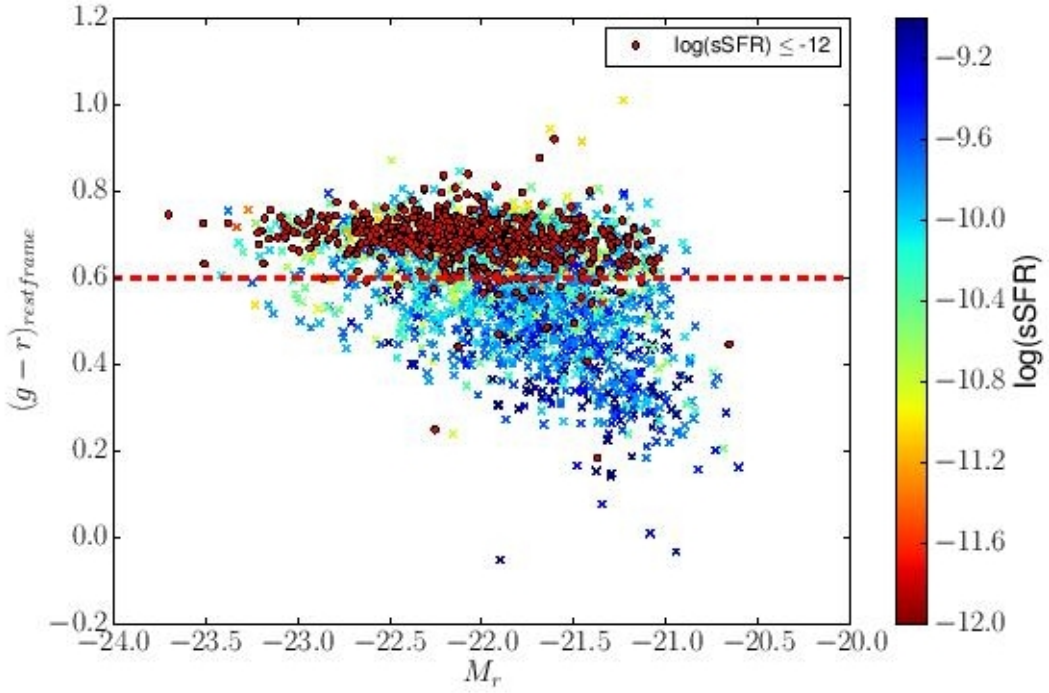

Fig. 5: Colour-magnitude diagram for galaxies in the magnitude-limited sample for the subset with both SINOPSIS and LePhare outputs. Red points indicate passive galaxies, while galaxies with log(sSFR)>-12 are colour-coded according to their sSFR. The red dotted line shows the separation between red and blue objects.

Таки да, в центрах скоплений меньше star-forming галактик!

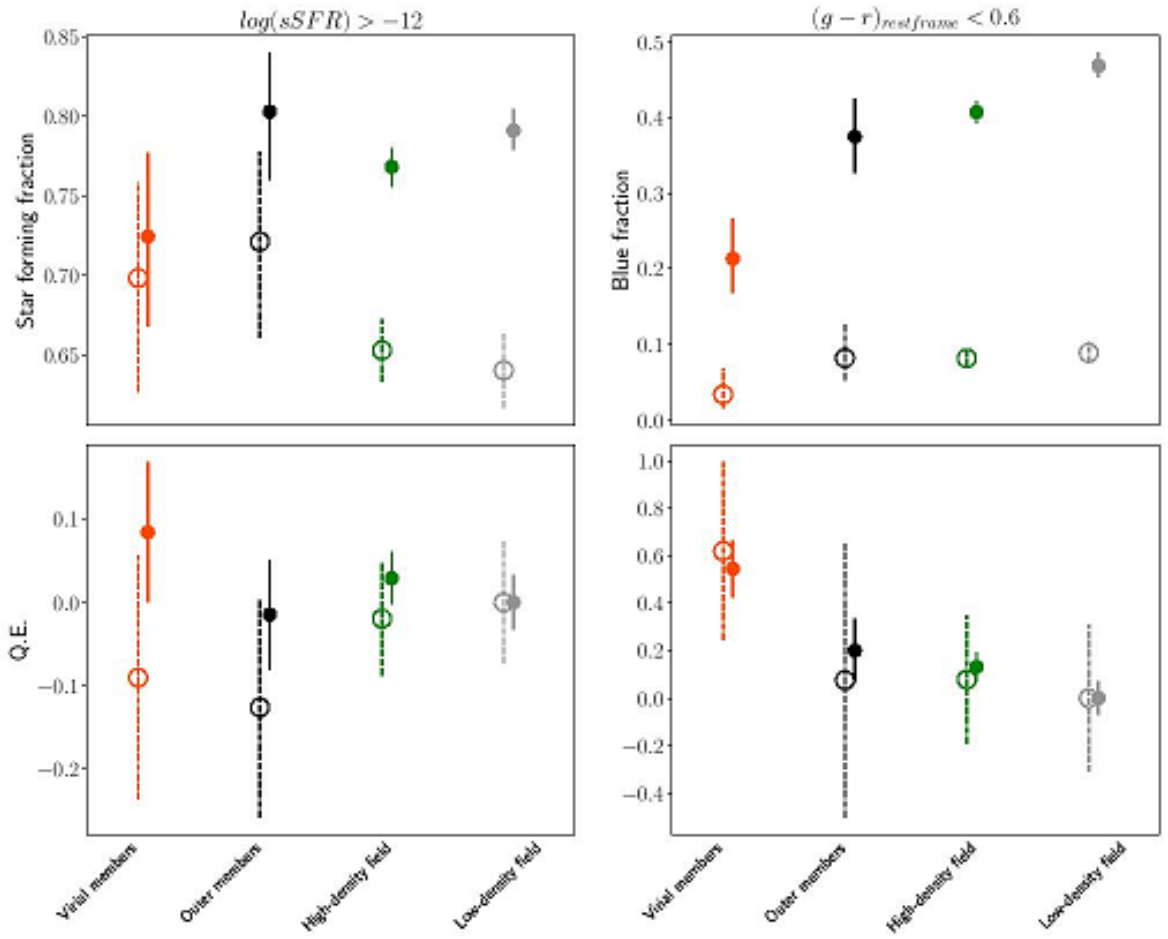

Fig. 6: Fraction of star-forming galaxies in different environments, computed with sSFR (left panel) and rest-frame colour (right panel). The fractions obtained using the magnitude-limited sample are represented with filled symbols and solid errors, those obtained using the mass-limited sample are represented by empty symbols and dashed error bars. Errors are derived by means of a bootstrap method. The two lower panels show the quenching efficiency (Q.E.) in different environments, computed with equation 3 for both the star-forming and blue samples. The Q.E. of field galaxies, which is by definition set to zero (see Eq. 3), is shown in both panels as a reference. The error bars on the Q.E of the low-density field depend on the amplitude of the confidence intervals associated with the fractions of star-forming and passive galaxies from bootstrapping.

И больше нет различия по типу окружения!

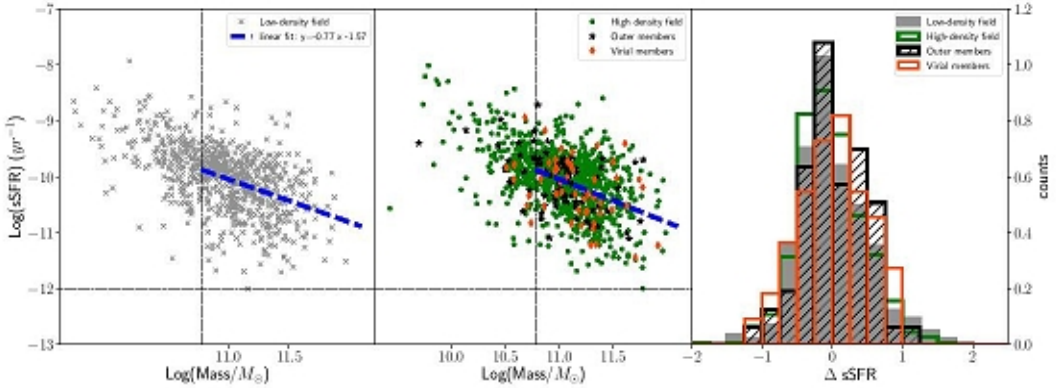

Fig. 7: Specific star formation rate (sSFR)–mass relation for galaxies in the low-density field (left panel), and galaxies in the high-density field and cluster virial and outer regions (green dots, orange diamonds, and black stars in the central panel). The vertical and horizontal lines show the stellar mass limit and our adopted separation between star-forming and passive galaxies. The blue dashed line is the fit to the relation of the sample including all the environments. The right panel shows the distribution of the differences between the galaxy sSFRs and their expected values according to the fit given their mass.

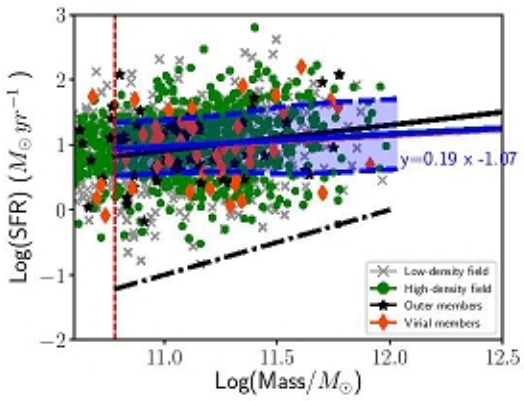

Fig. 8: SFR–mass relation for galaxies in the low-density field (grey crosses), in the high-density field (green dots), cluster virial (orange diamonds), and outer members (black stars). The red dashed vertical line shows the stellar mass limit. The blue line is the fit to the relation including all the environments, and the shaded areas correspond to 1σ errors on the fitting line. Linear fits for each environment are shown separately in the figure, colour-coded according to the legend. The black dashed line represents the log(sSFR)=-12 limit.

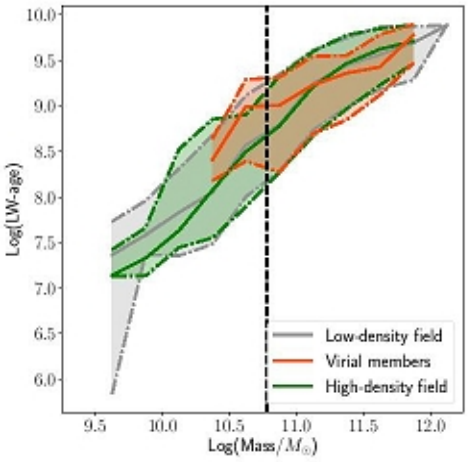

Fig. 9: Median luminosity-weighted age–mass relation computed in non-independent stellar mass bins for different environments, as shown in the legend. The stellar mass limit is shown with a vertical black dashed line. Shaded areas are the 32nd and 68th percentiles, corresponding to 1σ error bars.

1805.03903

MAGNETIC FIELDS IN THE GALACTIC HALO SUPPRESS FOUNTAIN-DRIVEN RECYCLING AND ACCRETION

Asger Grønnow,[1] Thor Tepper-García,[1] and Joss Bland-Hawthorn[1, 2]

[1] *Sydney Institute for Astronomy, School of Physics A28, The University of Sydney, NSW 2006, Australia*
[2] *Centre of Excellence for Astronomy in Three Dimensions (ASTRO-3D), Australia*

Submitted to Astrophysical Journal

ABSTRACT

The Galactic halo contains a complex ecosystem of multiphase intermediate-velocity and high-velocity gas clouds whose origin has defied clear explanation. They are generally believed to be involved in a Galaxy-wide recycling process, either through an accretion flow or a large-scale fountain flow, or both. Here we examine the evolution of these clouds in light of recent claims that they may trigger condensation of gas from the Galactic corona as they move through it. Specifically, we measure gas condensation along a cloud's wake, with and without the presence of an ambient magnetic field, using two- and three-dimensional, high-resolution Adaptive Mesh Refinement (AMR) simulations. We find that three-dimensional simulations are essential to capture the condensation even when no magnetic field is included. Magnetic fields significantly inhibit condensation in the wake of clouds at $t \gtrsim 25$ Myr, preventing the sharp upturn in cold gas mass seen in previous non-magnetic studies. The magnetic field suppresses the onset of the Kelvin-Helmholtz instability which is responsible for the ablation and consequent mixing of cloud and halo

Фиксируются параметры газа в гало и варьируются – в облаках

Table 1. Fixed simulation parameters

$v_{\mathrm{wind},x}$[a] (km s^{-1})	n_h (cm^{-3})	T_h K	$[\mathrm{Fe/H}]_\mathrm{h}$	r_c (kpc)	x (kpc)	y (kpc)	z (kpc)
75	10^{-3}	2×10^6	-0.5	0.1	$-0.6 \leq x \leq 0.6$	$-0.6 \leq y \leq 0.6$	$-2.0 \leq z \leq 10.0$

[a]This corresponds to a Mach number of 0.45.

Варьируются T(cloud) , n(cloud) , [Fe/H](cloud) , напряженность поля (3 варианта, 0, слабое, сильное)

Трехмерный расчет

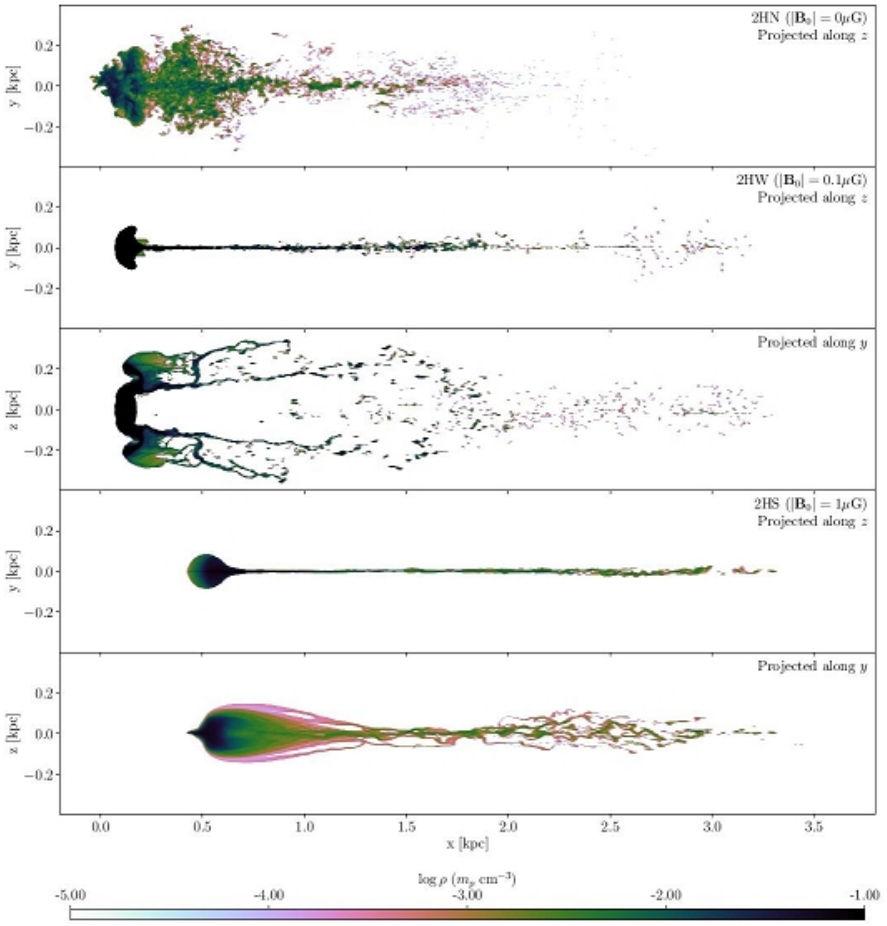

Figure 1. Projected mass density of cold ($T < 5 \times 10^5$ K) gas at the end of the simulations at $t \approx 50$ Myr for simulation 2HN (top, projected along the z-axis), simulation 2HW (second and third panels from the top, projected along the z-axis and the y-axis, respectively), and simulation 2HS (fourth and fifth panels from the top, projected along the z-axis and the y-axis, respectively). Because of the symmetry in the initial conditions the y-projection of the non-magnetic simulation (2HN) is similar to the z-projection and is therefore omitted. The cloud in simulation 2HS is at a different position compared to the other two cases because it has been significantly slowed by magnetic tension. The color coding indicates the value of the density in units of m_p cm^{-3} on a logarithmic scale, where m_p is the proton mass.

Привет Фратернали!

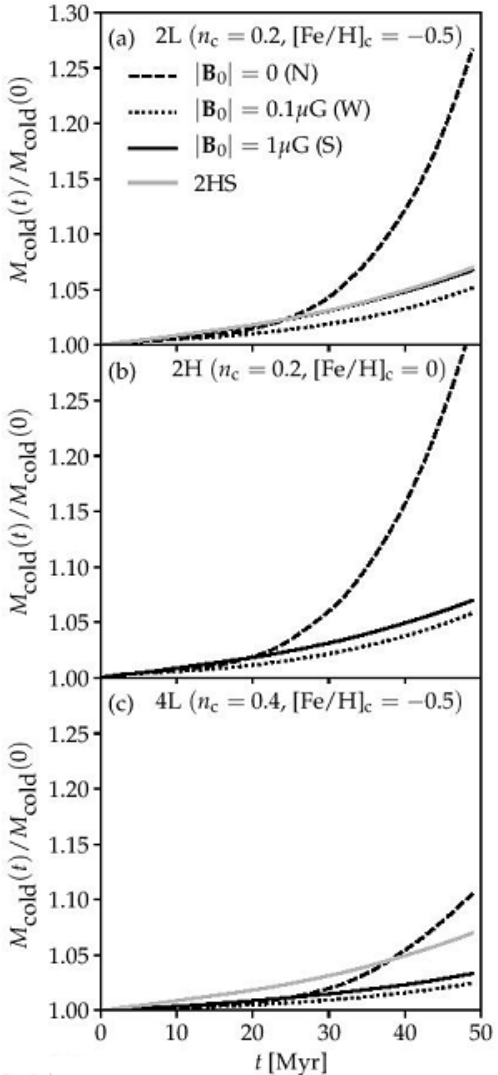

- Даже слабое поле подавляет остывание газа в «хвосте» летящего в гало сгустка из галактического фонтана. От скоростей и геометрии НЕ зависит.